

## SUPPLEMENTAL MATERIAL:

# A computational analysis of pro-angiogenic therapies for peripheral artery disease

### Supplemental Figures

**Fig S1.** Detailed response to biomaterial-based delivery of engineered VEGF constructs to the PAD Calf Muscle.

**Fig S2.** Efficacy of biomaterial-based VEGF delivery does not depend on endogenous VEGF splicing.

**Fig S3.** Detailed response to varying doses of “Covalent VEGF with Proteolysis” construct to the PAD Calf Muscle.

**Fig S4.** Additional metrics of response to gene therapy at Day 6 following treatment.

**Fig S5.** Detailed time-course response to gene therapy strategies.

**Fig S6.** Analysis of predicted VEGF<sub>165a</sub> and VEGF<sub>165b</sub> distribution in human body following VEGF-targeted antibody therapy.

**Fig S7.** Effect of VEGF-targeting antibodies on systemic free VEGF distribution.

**Fig S8.** Additional effects of VEGF-targeting antibodies on endothelial VEGFR2 signaling *in vivo*.

**Fig S9.** Effects of VEGF-targeting antibodies on endothelial total VEGFR2 ligation *in vivo*.

**Fig S10.** Effects of VEGF-targeting antibodies on endothelial cell surface VEGFR2 ligation *in vivo*.

**Fig S11.** Effects of VEGF-targeting antibodies on endothelial cell surface VEGFR1 ligation *in vivo*.

**Fig S12.** Relative antibody binding to VEGF<sub>165a</sub> and VEGF<sub>165b</sub> in the Main Body Mass and PAD Calf Muscle.

**Fig S13.** Comparison of VEGFR2 activation following biomaterial-based protein delivery, gene therapy, or anti-VEGF treatment.

### Supplemental References

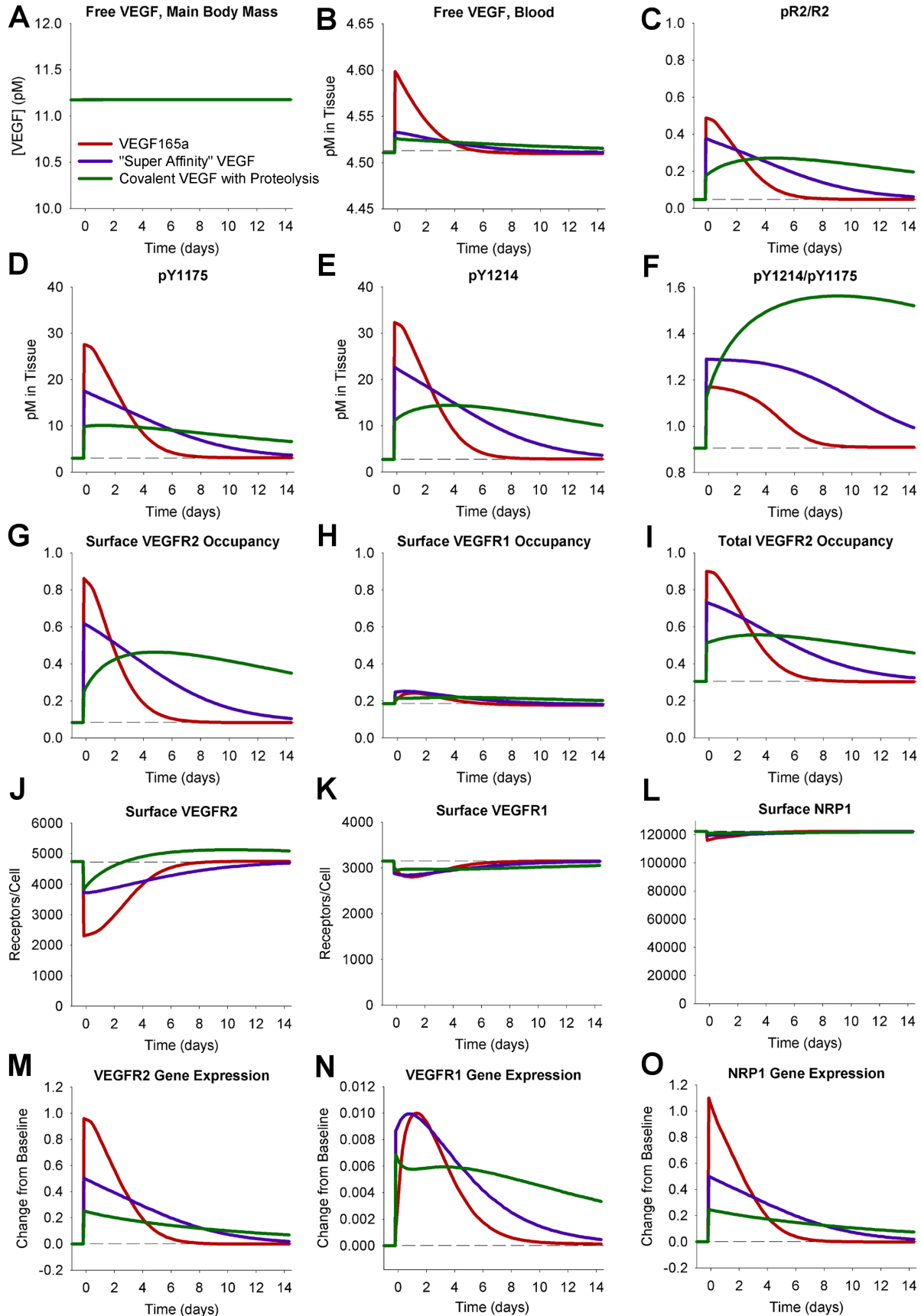


**Fig S1. Detailed response to biomaterial-based delivery of engineered VEGF constructs to the PAD Calf Muscle.** This figure is related to **Fig. 2** of the main manuscript. Free VEGF levels in other compartments (**A-B**), details of VEGFR2 phosphorylation (**C-F**), endothelial receptor occupancy (**G-I**), changes in surface receptor levels following treatment (**J-L**), and the dynamic changes in receptor production required to hold total receptor levels constant following treatment (**M-O**).

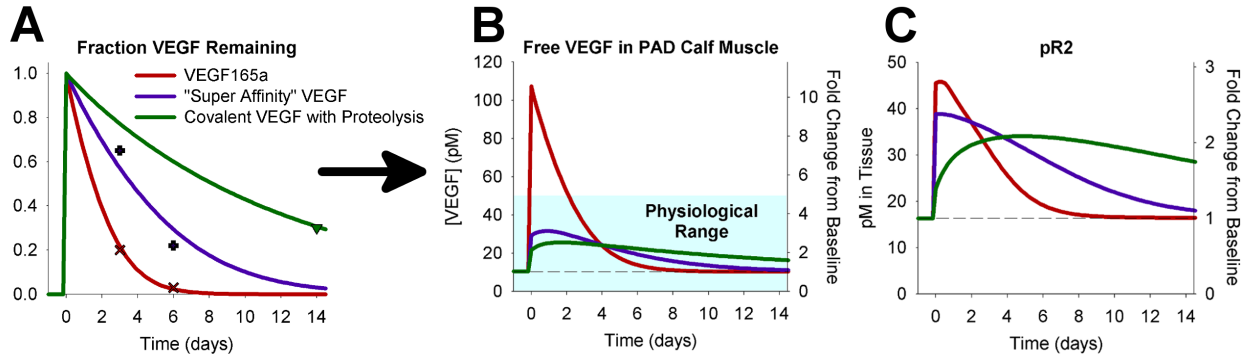


**Fig S2. Efficacy of biomaterial-based VEGF delivery does not depend on endogenous VEGF splicing.** This figure is related to **Fig. 2** of the main manuscript. Simulations of VEGF release from biomaterial (**A**), free VEGF in the PAD Calf Muscle (**B**), and VEGFR2 phosphorylation (**C**), with no endogenous secretion of VEGF<sub>165b</sub> (0%, all VEGF<sub>165a</sub>), as opposed to the case shown in **Fig. 2B**, with all VEGF<sub>165b</sub> (100%). All other conditions and dose size are the same as in **Fig. 2B**. Teal box indicates physiological range of VEGF expression, which typically varies no more than 3-5x in physiological and pathological conditions<sup>1</sup>.

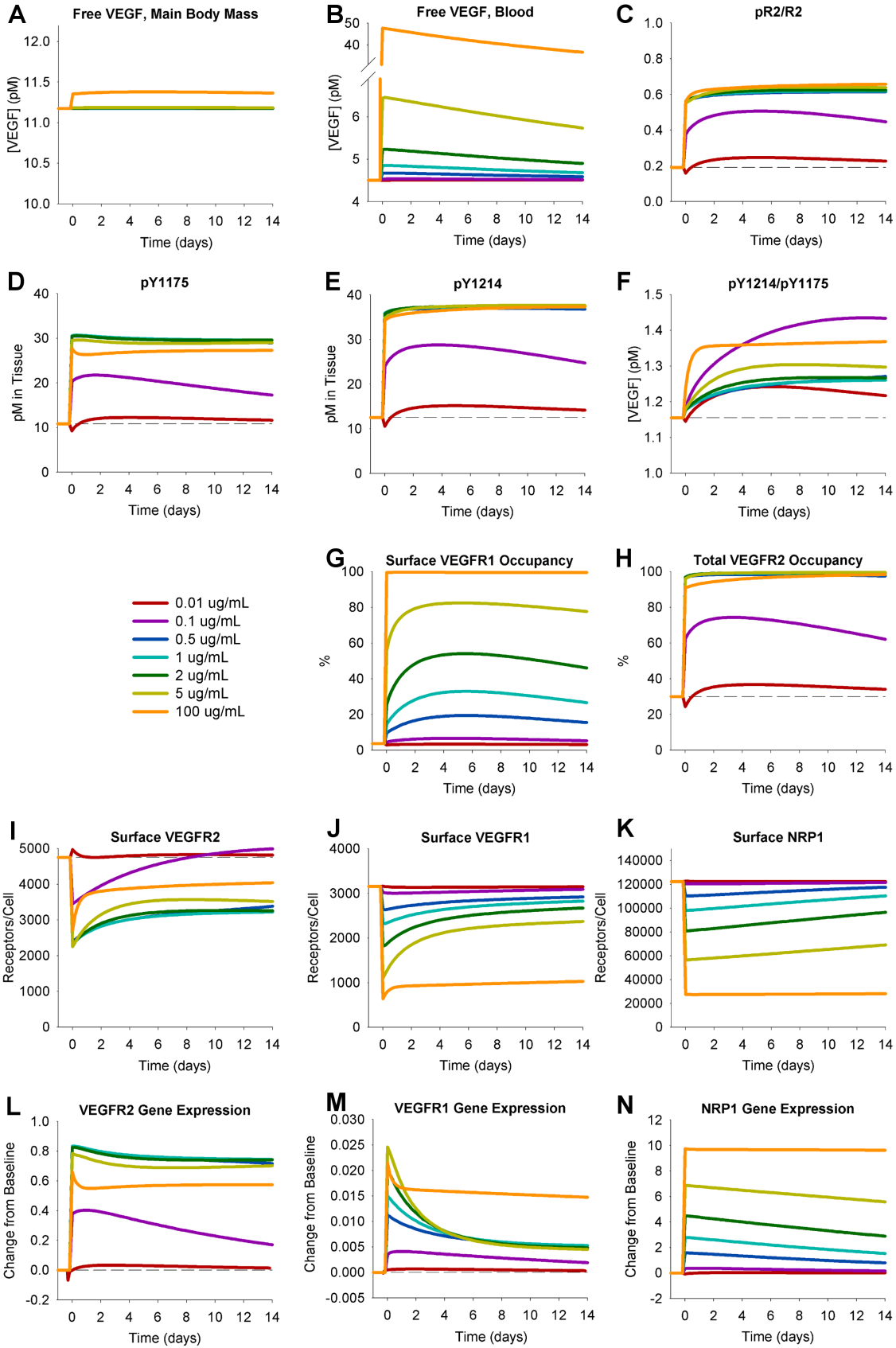


**Fig S3. Detailed response to varying doses of “Covalent VEGF with Proteolysis” construct to the PAD Calf Muscle.** This figure is related to **Fig. 2** of the main manuscript. Free VEGF levels in other compartments (**A-B**), details of VEGFR2 phosphorylation (**C-F**), endothelial receptor occupancy (**G-H**), changes in surface receptor levels following treatment (**I-K**), and the dynamic changes in receptor production required to hold total receptor levels constant following treatment (**L-N**).

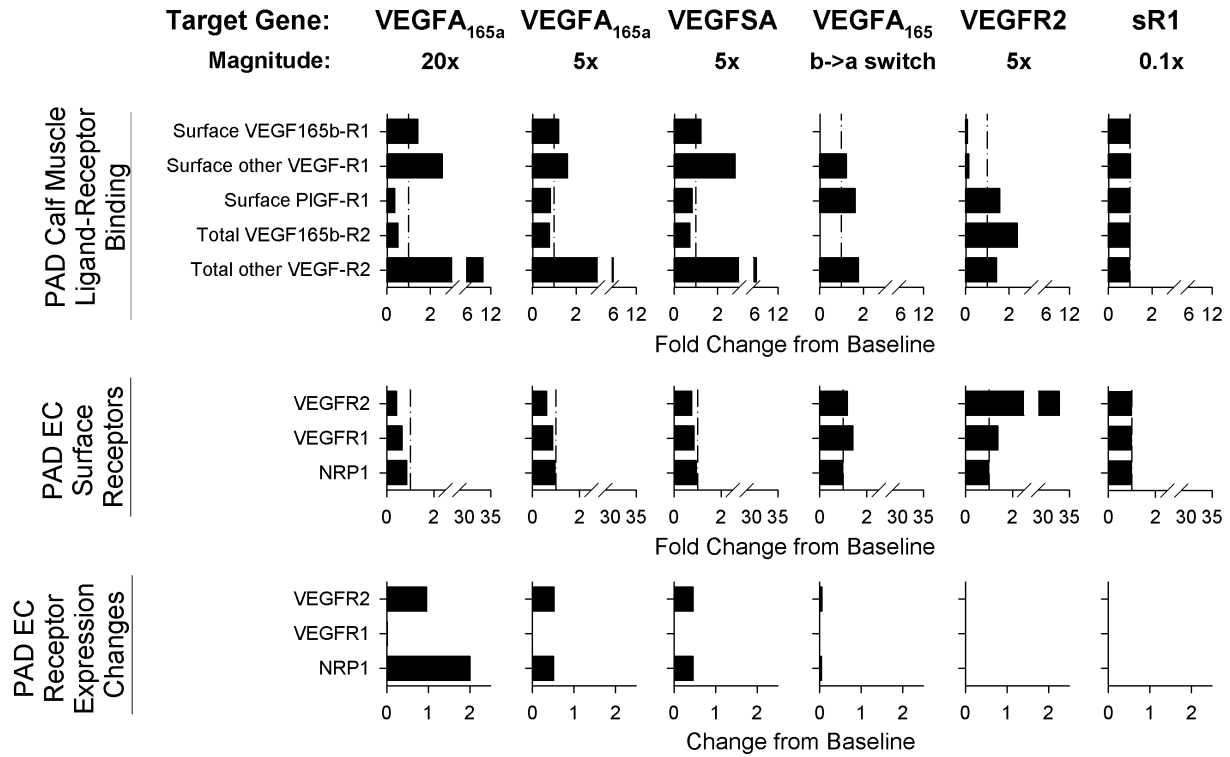


**Fig S4. Additional metrics of response to gene therapy at Day 6 following treatment.** This figure is related to **Fig. 3** of the main manuscript. Breakdown of ligands bound to VEGFR1 and VEGFR2 on endothelial cells (**top row**), endothelial surface receptor levels (**middle row**), and changes in receptor production required to hold total receptor levels constant 6 days post-treatment (**bottom row**).

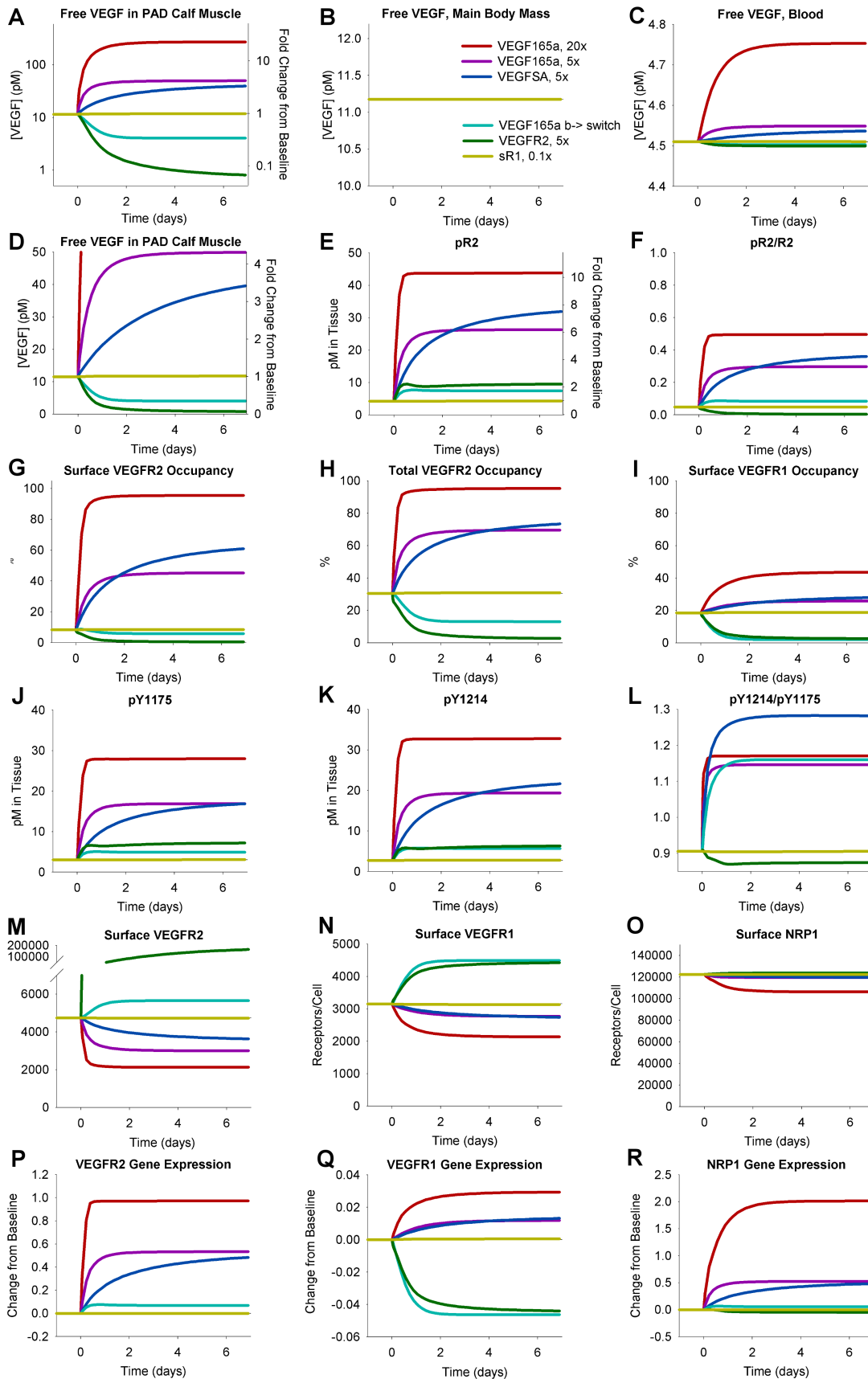


**Fig S5. Detailed time-course response to gene therapy strategies.** This figure is related to **Fig. 3** of the main manuscript. Free VEGF levels in other compartments (**A-D**), details of VEGFR2 phosphorylation (**E-F,J-L**), endothelial receptor occupancy (**G-I**), changes in surface receptor levels following treatment (**M-O**), and the dynamic changes in receptor production required to hold total receptor levels constant following treatment (**P-R**).

## Anti-VEGF

## Baseline

## Anti-VEGF<sub>165b</sub>

% of Local VEGF Production That Is VEGF<sub>165b</sub>

Main Body Mass: 100%

PAD Calf Muscle: 0%

Main Body Mass: 50%

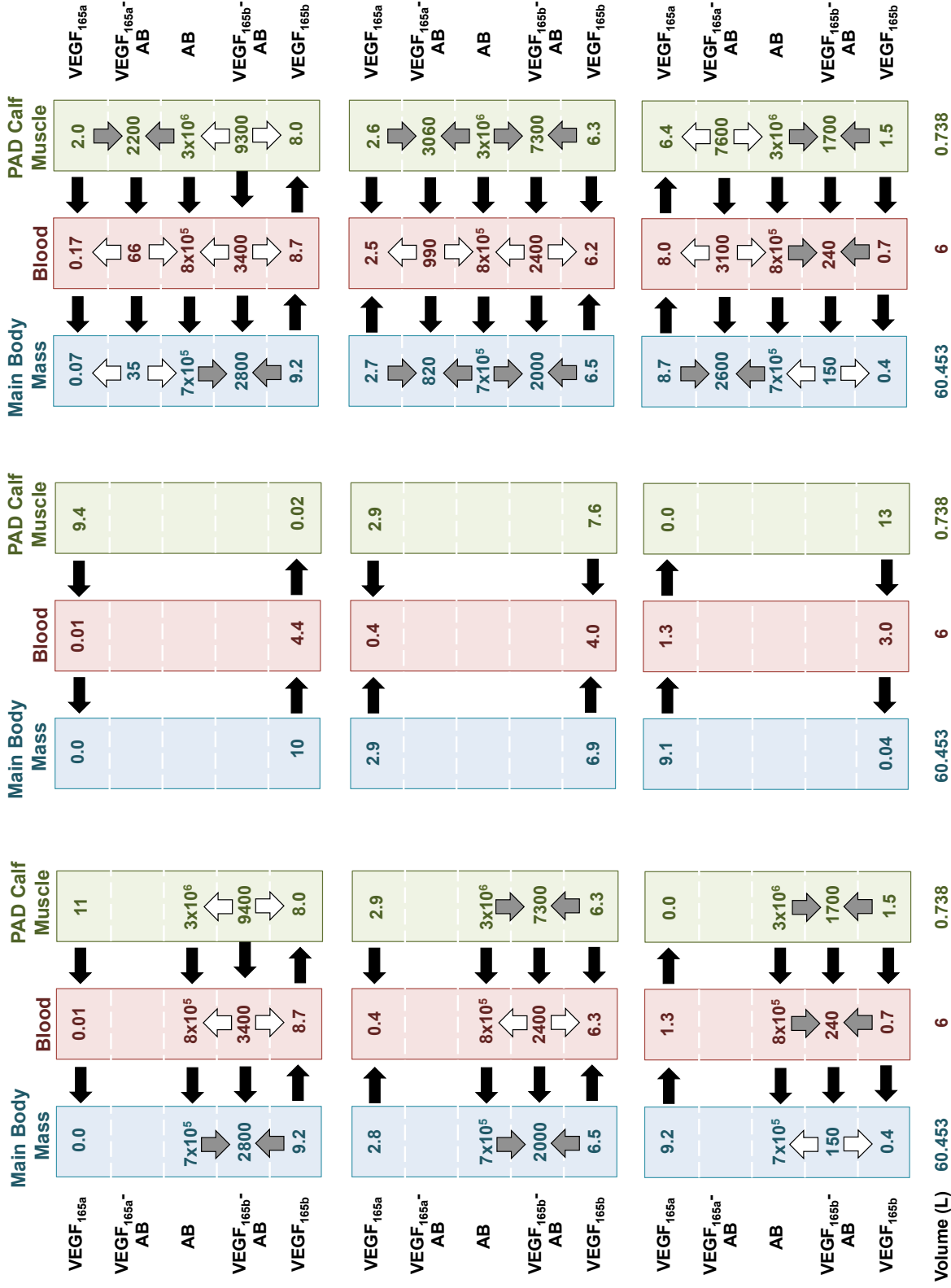
PAD Calf Muscle: 50%

Main Body Mass: 0%

PAD Calf Muscle: 100%

**Legend:**

- ↑ V-AB Association
- ⇄ V-AB Dissociation
- Vasc. Permeability
- All concentrations in pM.



Volume (L) 60.453 6 0.738 60.453 6 0.738 60.453 6 0.738

**Fig S6. Analysis of predicted VEGF<sub>165a</sub> and VEGF<sub>165b</sub> distribution in human body following VEGF-targeted antibody therapy.** This figure is related to **Fig. 5** of the main manuscript. Concentration of free VEGF<sub>165a</sub> and VEGF<sub>165b</sub>, free antibody, and VEGF-antibody complexes in the Main Body Mass, Blood, and PAD Calf Muscle at baseline (middle) and on Day 6 following IV infusion of anti-VEGF<sub>165b</sub> (left) or anti-VEGF (right), at different fractional VEGF<sub>165b</sub> secretion rates in the Main Body Mass and PAD Calf Muscle. Gray arrows indicate net association of antibody and VEGF, while white arrows denote net dissociation. Note that, while at baseline only local VEGF secretion is important for signaling, upon treatment with antibody, systemic effects become important (i.e. the concentrations of VEGF<sub>165a</sub> and VEGF<sub>165b</sub> in the other tissue compartment affect local VEGF levels). Changes in flow directions between compartments also occur following antibody treatment. Note that VEGF<sub>165b</sub> distribution is similarly impacted by both anti-VEGF<sub>165b</sub> and anti-VEGF; the difference in effect arises from the concomitant redistribution of VEGF<sub>165a</sub> by anti-VEGF.

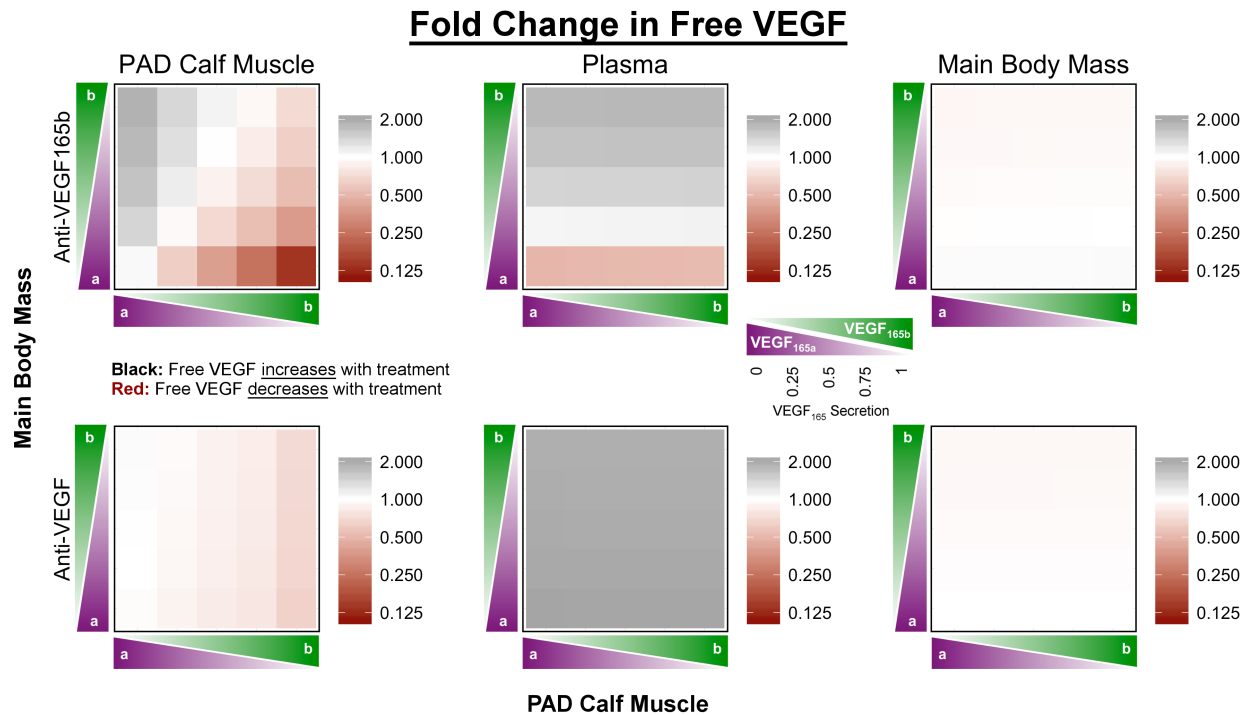


**Fig S7. Effect of VEGF-targeting antibodies on systemic free VEGF distribution.** This figure is related to **Fig. 5** of the main manuscript. Predicted fold change from baseline of total free VEGF in the PAD Calf Muscle (**left**), blood (**middle**) and Main Body Mass (**right**) on Day 6 following treatment with anti-VEGF<sub>165b</sub> (**top row**) or non-isoform-specific anti-VEGF (**bottom row**), as a function of the local fractional secretion of VEGF<sub>165b</sub> in the PAD Calf Muscle (x-axis) and the Main Body Mass (y-axis). Black indicates an increase in free VEGF, while red indicates a decrease.

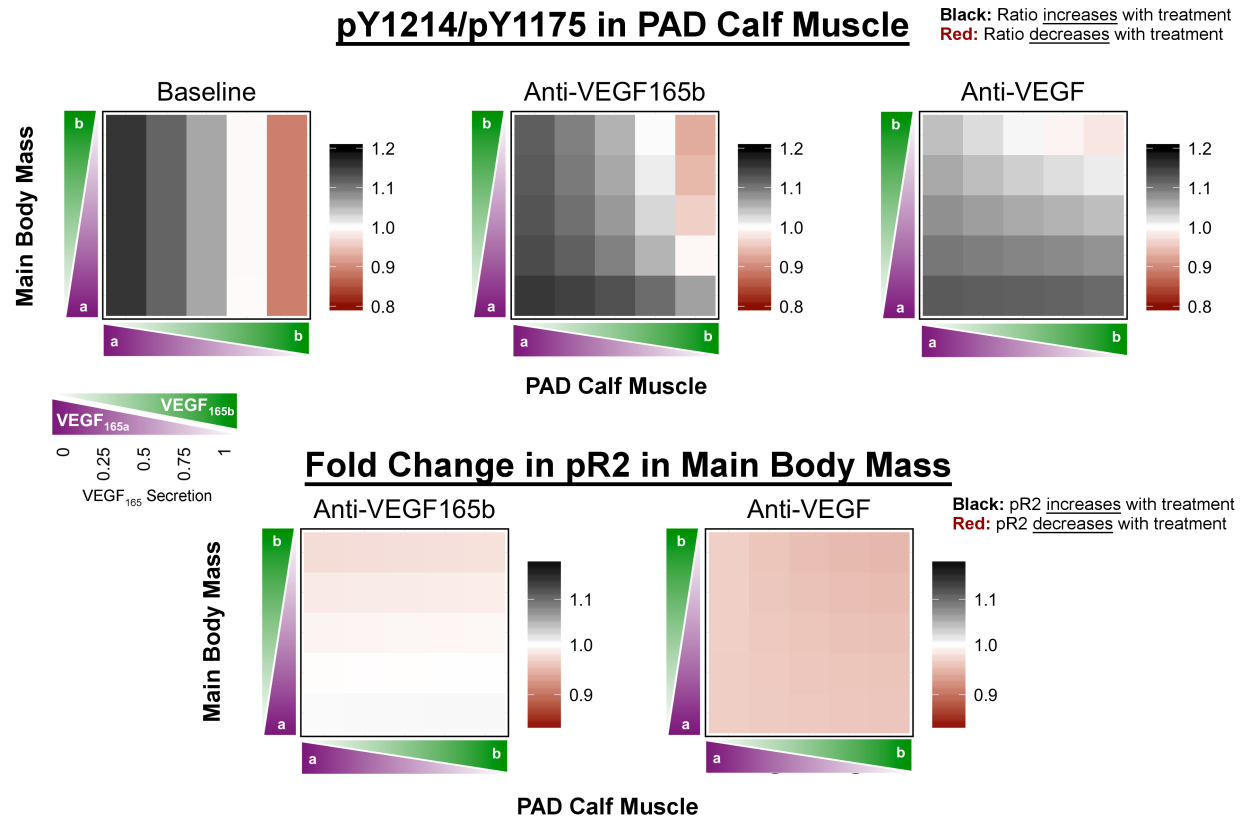


**Fig S8. Additional effects of VEGF-targeting antibodies on endothelial VEGFR2 signaling *in vivo*.** This figure is related to **Fig. 6** of the main manuscript. **Top:** Predicted ratio of VEGFR2 phosphorylation on Y1214 to Y1175 in the PAD Calf Muscle at baseline (**left**), and on Day 6 following treatment with Anti-VEGF<sub>165b</sub> (**middle**) or a non-isoform-specific Anti-VEGF (**right**), as a function of the local fractional secretion of VEGF<sub>165b</sub> in the PAD Calf Muscle (x-axis) and the Main Body Mass (y-axis). **Bottom:** Predicted fold change in VEGFR2 phosphorylation in the Main Body Mass on Day 6 following systemic antibody treatment. Black indicates an increase, while red indicates a decrease.

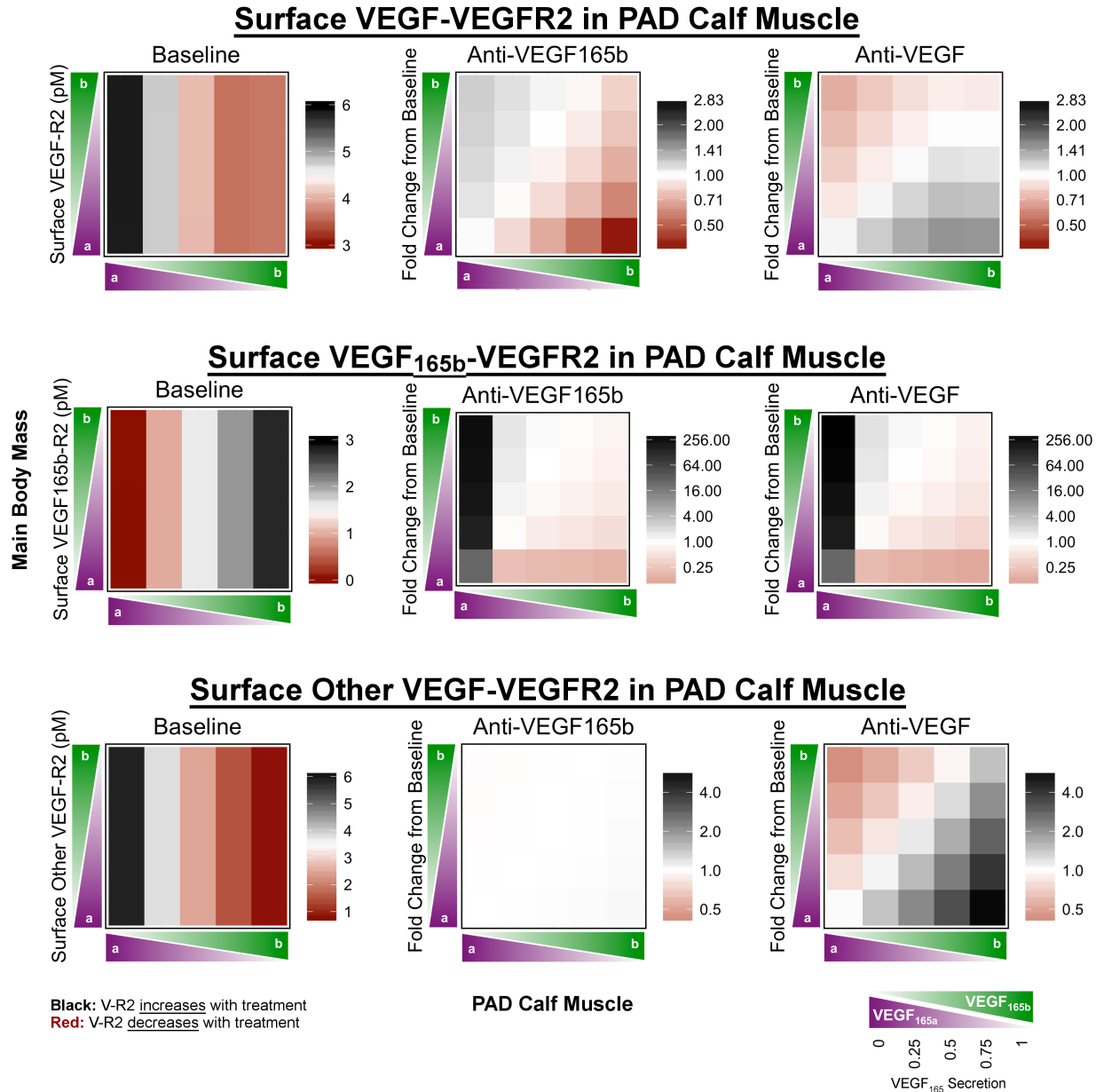


**Fig S9. Effects of VEGF-targeting antibodies on endothelial total VEGFR2 ligation *in vivo*.** This figure is related to **Fig. 6** of the main manuscript. Predicted total binding of VEGF to VEGFR2 (**top row**), VEGF<sub>165b</sub>-R2 (**middle row**), and binding of other VEGF isoforms to VEGFR2 (**bottom row**) in the PAD Calf Muscle at baseline (**left**), and fold change from baseline on Day 6 following treatment with Anti-VEGF<sub>165b</sub> (**middle**) or a non-isoform-specific Anti-VEGF (**right**), as a function of the local fractional secretion of VEGF<sub>165b</sub> in the PAD Calf Muscle (x-axis) and the Main Body Mass (y-axis). Black indicates an increase, while red indicates a decrease. Note differences in color scales by row.

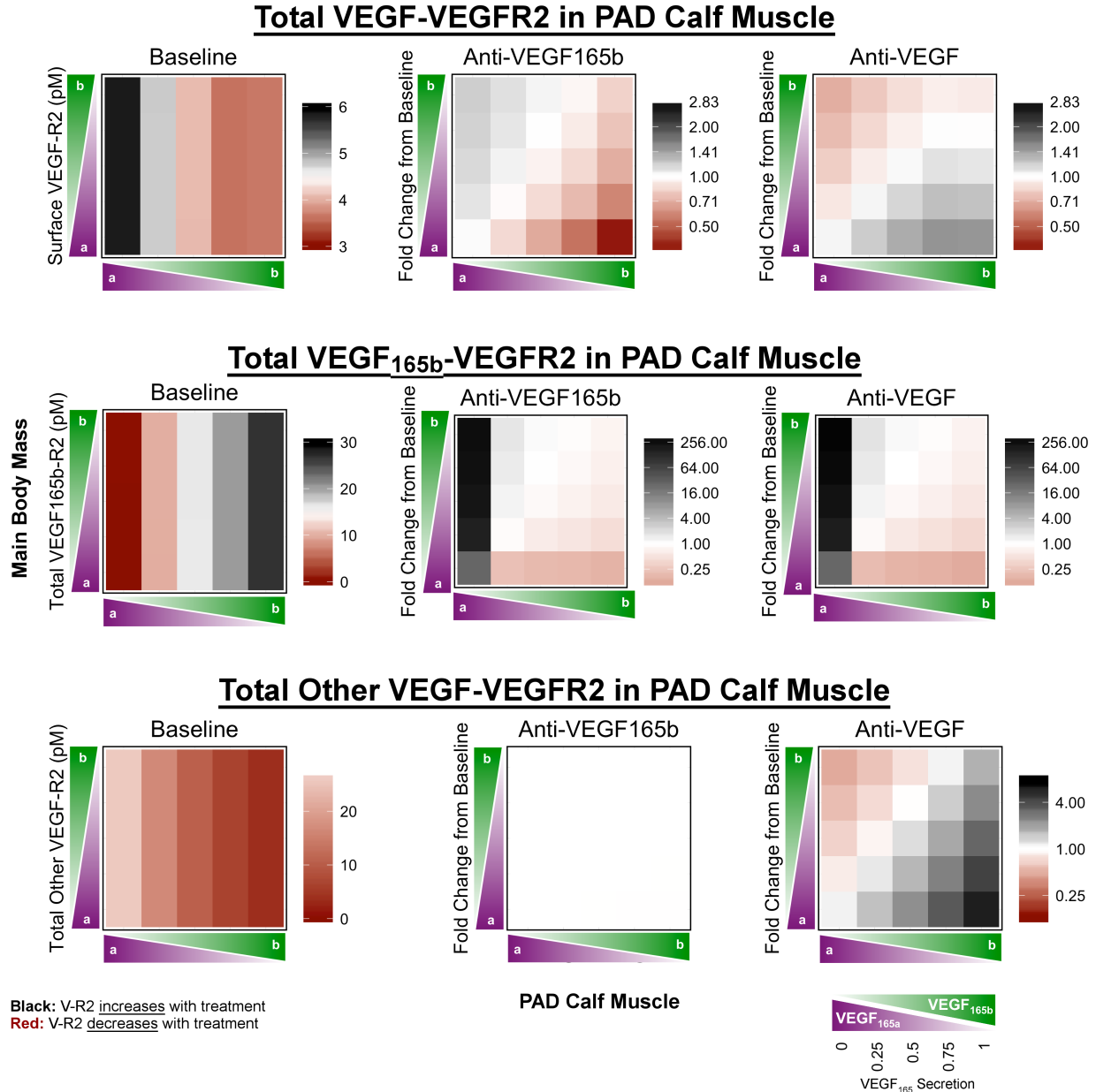


**Fig S10. Effects of VEGF-targeting antibodies on endothelial cell surface VEGFR2 ligation *in vivo*.** This figure is related to Fig. 6 of the main manuscript. Predicted total binding of VEGF to VEGFR2 (**top row**), VEGF<sub>165b</sub>-R2 (**middle row**), and binding of other VEGF isoforms to VEGFR2 (**bottom row**) in the PAD Calf Muscle at baseline (**left**), and fold change from baseline on Day 6 following treatment with Anti-VEGF<sub>165b</sub> (**middle**) or a non-isoform-specific Anti-VEGF (**right**), as a function of the local fractional secretion of VEGF<sub>165b</sub> in the PAD Calf Muscle (x-axis) and the Main Body Mass (y-axis). Black indicates an increase, while red indicates a decrease. Note differences in color scales by row. **Note:** Changes in total other VEGF binding to VEGFR2 following anti-VEGF<sub>165b</sub> treatment (bottom row, center) <1% (due to lack of competition between VEGF isoforms for binding to VEGFR2), which are not visible with the given scale.

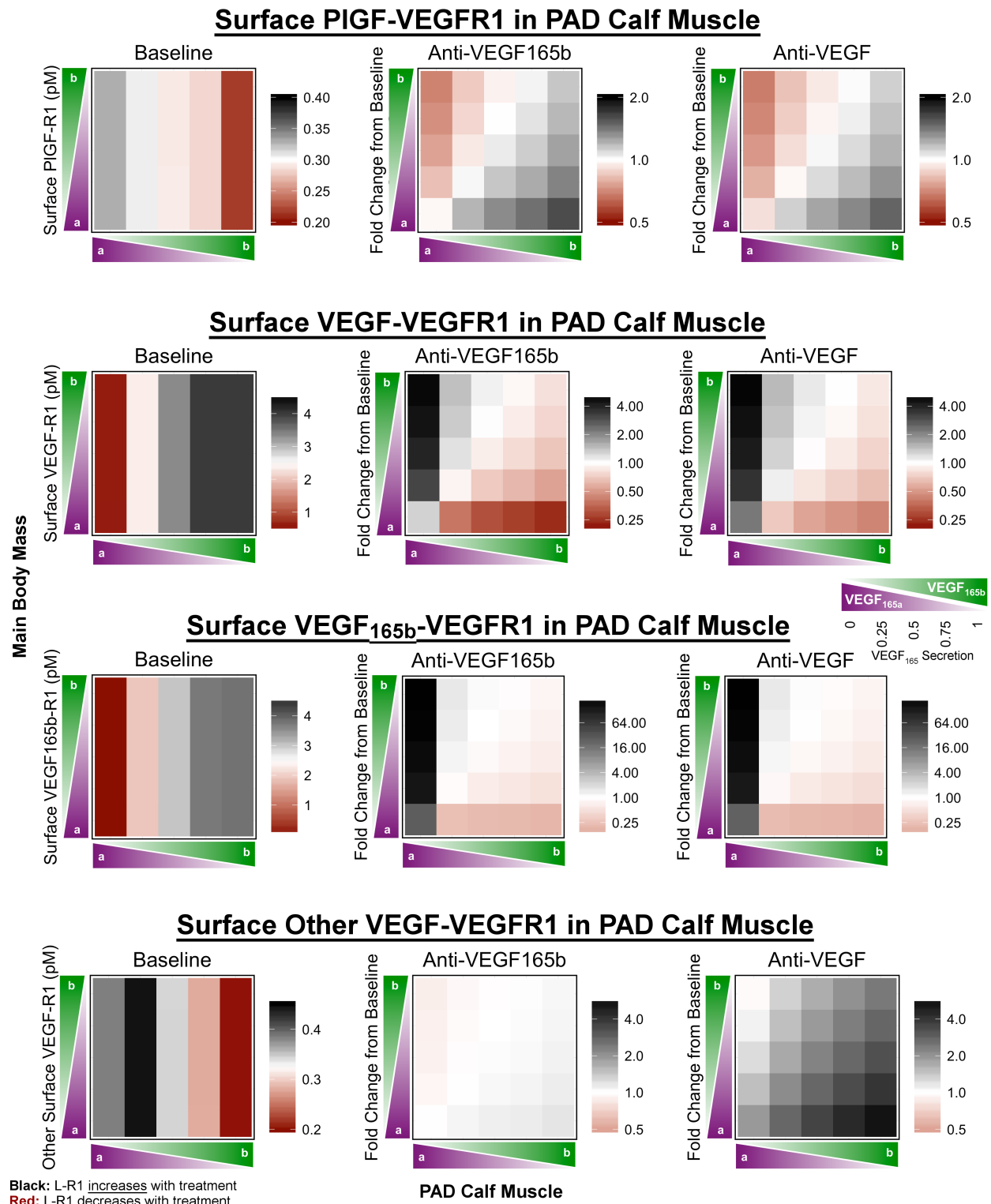
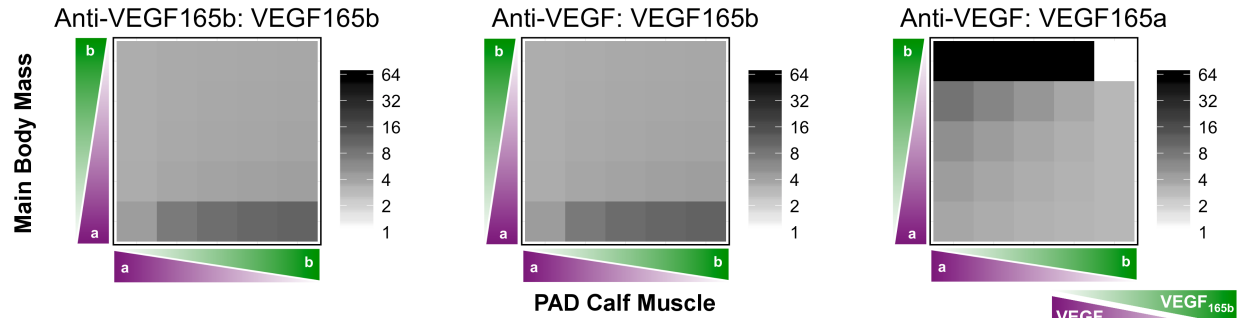


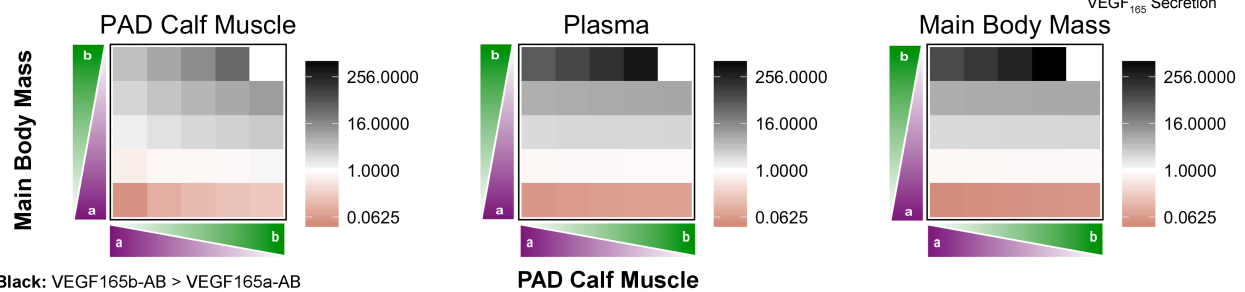
**Fig S11. Effects of VEGF-targeting antibodies on endothelial cell surface VEGFR1 ligation *in vivo*.** This figure is related to Fig. 6 of the main manuscript. Predicted total binding of PIGF to VEGFR1 (top row), total VEGF to VEGFR1 (2nd row), VEGF<sub>165b</sub>-R1 (3rd row), and binding of other VEGF isoforms to VEGFR1 (bottom row) in the PAD Calf Muscle at baseline (left), and fold change from baseline on Day 6 following treatment with Anti-VEGF<sub>165b</sub> (middle) or a non-

isoform-specific Anti-VEGF (**right**), as a function of the local fractional secretion of VEGF<sub>165b</sub> in the PAD Calf Muscle (x-axis) and the Main Body Mass (y-axis). Black indicates an increase in Free VEGF, while red indicates a decrease. Note differences in color scales by row.

## Ratio of VEGF Bound to Antibody in PAD Calf Muscle vs. Main Body Mass



## Ratio of VEGF<sub>165b</sub> to VEGF<sub>165a</sub> Bound to Anti-VEGF



Black: VEGF<sub>165b</sub>-AB > VEGF<sub>165a</sub>-AB  
 Red: VEGF<sub>165b</sub>-AB < VEGF<sub>165a</sub>-AB

**Fig S12. Relative antibody binding to VEGF<sub>165a</sub> and VEGF<sub>165b</sub> in the Main Body Mass and PAD Calf Muscle.** This figure is related to Fig. 5 of the main manuscript. **Top:** Predicted ratio of VEGF bound to the antibody in the PAD Calf Muscle as compared to the Main Body Mass on Day 6 following treatment, as a function of the local fractional secretion of VEGF<sub>165b</sub> in the PAD Calf Muscle (x-axis) and the Main Body Mass (y-axis). Left: VEGF<sub>165b</sub> bound to Anti-VEGF<sub>165b</sub>; Middle: VEGF<sub>165b</sub> bound to Anti-VEGF; Right: VEGF<sub>165a</sub> bound to Anti-VEGF. **Bottom:** Predicted ratio of VEGF<sub>165b</sub> to VEGF<sub>165a</sub> bound to Anti-VEGF in the PAD Calf Muscle (**left**), Blood (**middle**), and Main Body Mass (**right**) at Day 6 following treatment. In most cases, VEGF<sub>165b</sub> dominates due to its over-representation relative to its secretion fraction. Black indicates a ratio >1, while red indicates a ratio <1.

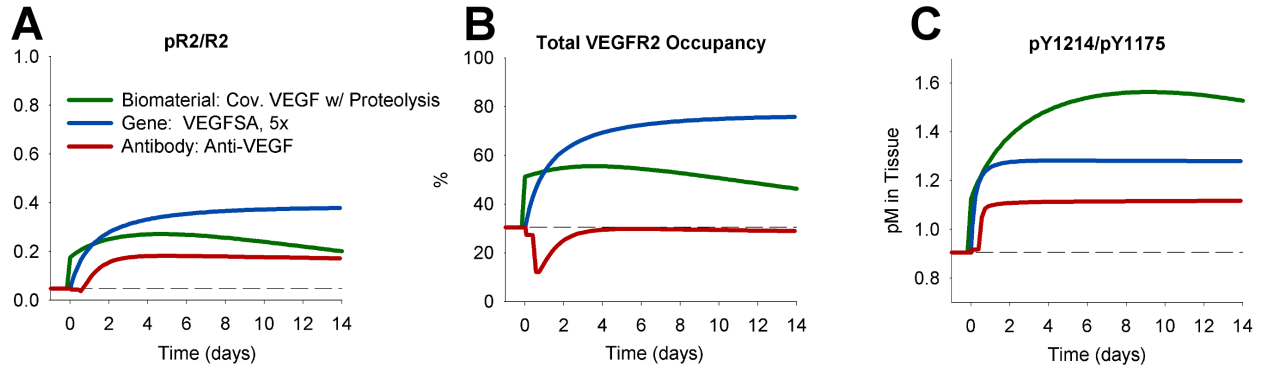


**Fig S13. Comparison of VEGFR2 activation following biomaterial-based protein delivery, gene therapy, or anti-VEGF treatment.** This figure is related to Fig. 7 of the main manuscript. Fraction of total VEGFR2 phosphorylated (**A**), total VEGFR2 occupancy (**B**), and pY1214/pY1175 (**C**) over time following treatment induction.

### **Supplemental References**

1. Kut C, Mac Gabhann F, Popel AS. Where is vegf in the body? A meta-analysis of vegf distribution in cancer. *British Journal of Cancer*. 2007;97:978-985